



HAL
open science

Advanced TCAD modeling of HfO₂-based ReRAM: coupling redox reactions and thermal effects

Youssef Hirchaou, Wolfgang Goes, Carl Hylin, Philippe Blaise, Jing Li,
François Triozon

► **To cite this version:**

Youssef Hirchaou, Wolfgang Goes, Carl Hylin, Philippe Blaise, Jing Li, et al.. Advanced TCAD modeling of HfO₂-based ReRAM: coupling redox reactions and thermal effects. SISPAD 2023 - Conference on Simulation of Semiconductor Processes and Devices, Sep 2023, Kobe, Japan. pp.333-336, 10.23919/SISPAD57422.2023.10319635 . cea-04555874

HAL Id: cea-04555874

<https://cea.hal.science/cea-04555874>

Submitted on 23 Apr 2024

HAL is a multi-disciplinary open access archive for the deposit and dissemination of scientific research documents, whether they are published or not. The documents may come from teaching and research institutions in France or abroad, or from public or private research centers.

L'archive ouverte pluridisciplinaire **HAL**, est destinée au dépôt et à la diffusion de documents scientifiques de niveau recherche, publiés ou non, émanant des établissements d'enseignement et de recherche français ou étrangers, des laboratoires publics ou privés.

Advanced TCAD Modeling of HfO₂-based ReRAM: Coupling Redox Reactions and Thermal Effects

Y. Hirchaou^{1,2}, W. Goes¹, C. Hylin¹, P. Blaise¹, J. Li², F. Triozon²

¹Silvaco-France, 38330 Montbonnot Saint-Martin, France, email: youssef.hirchaou@silvaco.com

²Univ. Grenoble Alpes, CEA, LETI, F-38000 Grenoble, France, francois.triozon@cea.fr

Abstract—This paper presents a TCAD modeling approach for HfO₂-based ReRAM (Resistive Random Access Memory). For describing the switching and retention behaviors of a ReRAM cell, the proposed model includes the essential redox reactions coupled to an electron transport model and to heat generation. The effects of various parameters such as applied voltage, sweep time, and device geometry on the switching behavior are investigated. Simulation results demonstrate that thermal management is crucial both for the reliable operation of ReRAM cells and retention. The proposed TCAD model provides insight into the design and optimization of HfO₂-based ReRAM devices.

I. INTRODUCTION

Oxide-based resistive random access memory (OxRAM) is a promising technology for embedded non-volatile memory devices. Due to the widespread use of HfO₂ in complementary metal-oxide-semiconductor (CMOS) fabrication, OxRAMs can be easily integrated into CMOS technology. In addition, OxRAMs offer low energy consumption and the potential to be used as multilevel memories for neuromorphic neural networks. While kinetic Monte Carlo (KMC) simulations [1] have advanced the understanding of OxRAMs, faster tools, such as TCAD simulations, appear necessary for device design engineering. In this article, we present a complete TCAD model that incorporates the relevant electrochemistry coupled with thermal effects to explain the switching and retention behaviors of OxRAMs.

II. MODEL DESCRIPTION

The model is developed within the Victory Device simulator [2]. We describe a TiN/HfO₂/Ti stack schematized in Fig. 1, where the top electrode (TE) made of Ti can react with oxygen ions moving in the oxide. A cylindrical symmetry around a nanometric conductive filament (CF) is assumed, allowing a 2D description. The oxide layer has a typical thickness of a few nm and a radius of a few tens of nm. The OxRAM is connected in series with a compliance transistor described by a compact model. The species concentrations within the oxide and their reactions with the TE interface are described by continuous functions evolving through drift-diffusion and chemical kinetics equations. A non-stoichiometric oxide includes a large number of lattice defects that preferentially occur in clusters and can carry small currents. In our model, they are represented by the so-called weak spots D_{ws} and are assumed to decrease laterally according to a Gaussian distribution as shown in Fig. 1. Upon the application of large electric fields, the D_{ws} can undergo a field-dependent forming reaction $D_{ws} \rightleftharpoons V_O^{2+} + I_O^{2-}$ where they dissociate into oxygen vacancies V_O^{2+} and oxygen interstitials I_O^{2-} . The V_O are immediately neutralized by electron capture or emission process as in [3] and become immobile in their neutral charge state due to a high diffusion barrier. Due to the capture and emission processes, the reaction equation effectively modifies to $D_{ws} + 2e^- \rightleftharpoons V_O + I_O^{2-}$. The negatively charged I_O^{2-} are moving due to diffusion or drift under an electric field. They can also react with the interface of the active electrode, represented by the redox equation $T_{If} + I_O^{2-} \rightleftharpoons T_{IfO} + 2e^-$, where T_{IfO} and T_{If} denote the oxidized and reduced interface sites, respectively. The chemistry is described by the equations shown in Tab. I. In addition, our model accounts for the charges in the Poisson equation, the heat generation in the lattice heat flow equation, and the electron transport in the electron drift-diffusion equation using the phenomenological bridging mobility model [4]. The main parameters used in our simulations are listed in Tab. II. Note that the forming of the conductive filament is not simulated, but obtained by imposing a high initial concentration of weak spots D_{ws} , and by equilibrating the system of chemical species using a transient simulation. In the following, the SET, RESET, and retention are investigated, with triangular voltage pulses applied for SET and RESET.

III. SIMULATION RESULTS

SET phase: At the beginning of this phase, a small current is carried by the highly defective region within the oxide, associated

with the high-resistance state (HRS). It gives rise to heat generation and substantially increases the temperature within the oxide, as shown in Fig. 3. Together with the increasing electric field across the oxide, the field-dependent forming reaction is initiated, which generates V_O and I_O^{2-} . The V_O vacancies allow for trap-to-trap tunneling through the oxide and forms the CF associated with the low-resistance state (LRS). The resulting V_O concentration is shown in Fig. 2. The I_O^{2-} drift towards the interface of TE, where they bond to interface sites T_{If} . Even though this interface reaction has a relatively high energy barrier, it can be overcome due to the high electric field and high temperatures. During the subsequent SET backward phase, the CF remains stable since the I_O^{2-} are effectively locked at the interface and are unavailable for the reverse mode of the forming reaction.

RESET phase: During this phase, the negative bias applied to the TE is gradually increased, causing an increase in current and heat generation, similar to the SET forward phase. The reverse mode of the interface reaction is activated due to the opposite polarity of the electric field and the higher device temperature. The electric field pushes the I_O^{2-} towards the interface of the inert bottom electrode (BE), where they recombine with the V_O to form weak spots again. This causes a rupture of the CF and switches the OxRAM device back to its HRS. During the RESET backward phase, the increasing amount of I_O^{2-} released dissolves the disrupted CF.

Cycling: The current-voltage hysteresis for a SET-RESET cycle is shown for different oxide thicknesses in Fig. 4 and different sweep times in Fig. 5. The SET and RESET voltage increase with larger oxide thicknesses. Since the electric field inside the oxide is reduced by a larger oxide thickness, larger applied voltages are required to initiate the forming and the interface reactions during the SET and the RESET phase of the current hysteresis. In agreement with experiments, our model also predicts an increase in the SET and RESET voltage with shorter sweep times.

Retention: The retention in the SET state is simulated by probing the current at 0.1 V at different temperatures, see Fig. 6. The retention of the SET state is assessed using long transient simulation at different temperatures, during which the current is probed at 0.1 V (see Fig. 6).

IV. DISCUSSION

One major challenge in the modeling of OxRAMs is that time constants span a wide range from μ s at an ambient temperature of 300K during resistive switching, up to 10^6 s for retention at around 500K. In a previous TCAD model [5], the wide range of time constants has been achieved by introducing empirical catalyst species, which accelerate the interface reaction at high fields. In this study, however, we focus on modeling the thermal effects, such as the thermal interface conductance [6]. As a result, the OxRAM devices can heat up to 900 K in agreement with the findings in [6]. As shown in Fig. 3, the highly defective region can cause a substantial heat-up of the device during the SET as well as the RESET phase. The increased temperatures effectively activate the interface reaction and thereby allow resistive switching down to the microsecond regime. However, the LRS after the SET phase remains stable up to 10^3 s at almost 500 K, as typically observed in retention experiments.

V. CONCLUSION

We have developed a quantitative TCAD model, including the key physical and chemical mechanisms in the resistive switching of OxRAM devices. A special focus has been put on simulating the self-heating effect, which allows for resistive switching in the μ s regime at room temperature and the long retention up to hours at 500 K. In addition, the model has been demonstrated to predict the trends for different oxide thicknesses and sweep times seen in experiments.

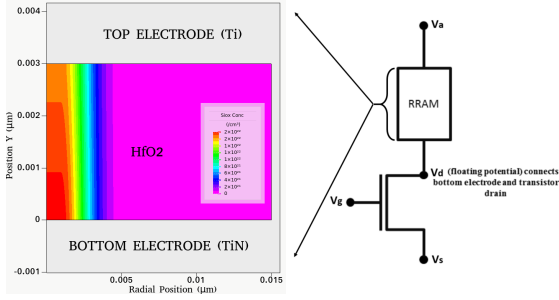


Fig. 1: Schematic of the simulated OxRAM device. (Left) Initial concentration of weak spots D_{ws} in cylindrical symmetry leading to the OxRAM switching. (Right) Applied voltages in a 1T1R structure with a current compliance.

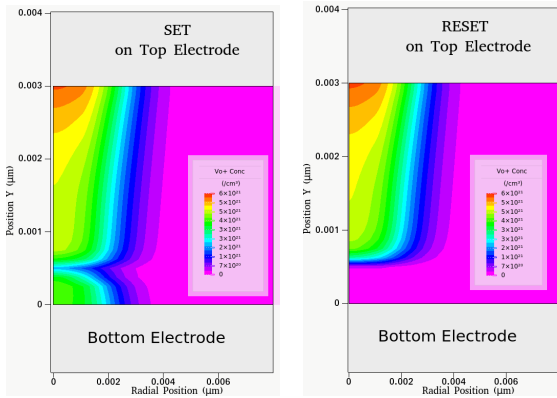


Fig. 2: OxRAM switching: V_O vacancies in the filamentary region. (Left) SET with a typical hourglass repartition. (Right) RESET, the conductive filament is broken close to the bottom electrode.

Poisson	$\nabla(\epsilon_r \epsilon_0 \nabla \varphi) = -q_0(n + \sum_i z_{X_i} [X_i])$
Species Cont.	$\partial_t X_i = D_{X_i} \left\{ \left(\frac{z_{X_i} q_0}{k_B T} [X_i] \nabla \varphi + \nabla [X_i] \right) \right\} + (G_{X_i} - R_{X_i})$ $R_{D_{ws}} = G_{V_O} = G_{I_O} = k_{bf} [D_{ws}] \exp(- (E_{bf} \pm d_{bf} \cdot E) / (k_B T))$ $G_{D_{ws}} = R_{V_O} = R_{I_O} = k_{br} [V_O] [I_O] \exp(- (E_{br} \mp d_{br} \cdot E) / (k_B T))$ $R_{T_{I_{FO}}} = G_{T_{I_f}} = G_{I_O} = k_{if} [T_{I_{FO}}] \exp(- (E_{if} \pm d_{if} \cdot E) / (k_B T))$ $G_{T_{I_{FO}}} = R_{T_{I_f}} = R_{I_O} = k_{ir} [T_{I_f}] [I_O] \exp(- (E_{ir} \mp d_{ir} \cdot E) / (k_B T))$
Heat flow	$C \partial_t T = \nabla \cdot (\kappa \nabla T) + (J_n \cdot E)$ with interface cond. $q_{ij} = G(T_i - T_j)$

Tab. I: Subset of equations used in the simulations. The electrostatics is described by the Poisson equation including the electron concentration n and the ionic charges $z_{X_i} [X_i]$ given by the product of the charge per a single species ion with the corresponding species concentration $[X_i]$. n is coupled to the electron drift-diffusion equation, which phenomenologically describes the conductivity of the CF based on the bridging mobility model [4]. The chemistry is described by the species continuity equations where $X_i = V_O, I_O, D_{ws}, T_{I_f}$, and $T_{I_{FO}}$. D_{X_i} is the corresponding species diffusivity using the Mott-Gurney model, which accounts for the field-dependence of the diffusion barriers. All species apart from the I_O^{2-} are assumed to be immobile so that their corresponding flux terms vanish and their continuity equations are determined by the corresponding reaction rates. E_{bf} and E_{br} are the forward and the reverse barrier of the forming reaction at zero field. These barriers are lowered or lifted according to the polarity of electric field $E = -\nabla \varphi$. The corresponding dipole moments d_{bf} and d_{br} are of the form $(2 + \epsilon_r)/3 \cdot x \cdot z_{X_i} \cdot p_0$ and $(2 + \epsilon_r)/3 \cdot (1 - x) \cdot z_{X_i} \cdot p_0$, respectively. $(2 + \epsilon_r)/3 \cdot p_0$ corresponds to the polarization factor with ϵ_r the dielectric constant and x specifies the location of the saddle point of the barrier as a fraction of the reaction coordinate. Analogous considerations hold for the continuity equations of the species T_{I_f} and $T_{I_{FO}}$. The heat flow equation includes a Joule heating term as in [7] in order to account for the self-heating effects. C and κ are the heat capacity and the heat conductivity, respectively. G denotes the interface thermal conductance.

Oxide V_O Generation	$E_{bf} = 1.4$ eV, $E_{br} = 0.2$ eV, $p_0 = 0.8$ q ₀ ·nm [8]
Interface I_O^{2-} Release	$E_{if} = 1.2$ eV, $E_{ir} = 0.7$ eV, $p_0 = 0.6$ q ₀ ·nm [8]
Oxide Thermal Conductivity	$\kappa = (0.04 + 0.0004 \times T)$ W/cm.K
Interface Thermal Conductance	$G_{th} = (10^4 + 10 \times T)$ W/cm ² .K

Tab. II: Physical parameters for the HfO₂-based OxRAM simulation, see text and table I for their meanings and references therein.

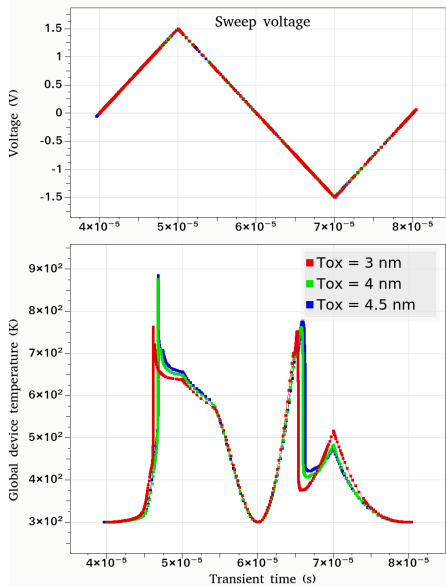


Fig. 3: Temperature profile during SET and RESET cycles. SET goes from 40 μs to 50 μs, RESET from 60 to 70 μs.

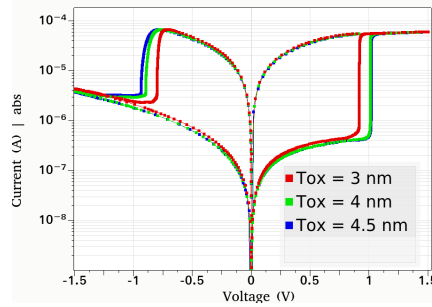


Fig. 4: Effect of different oxide thicknesses on the hysteresis curve, voltage is ±1.5V, 10 μs sweep time

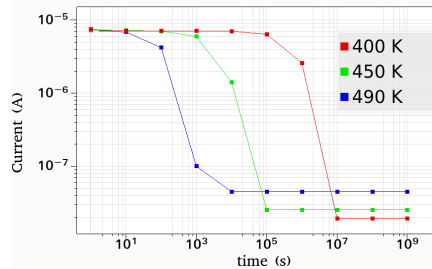


Fig. 6: SET retention: current probe at voltage $V = 0.1$ V and different times for $T = 400, 450,$ and 490 K.

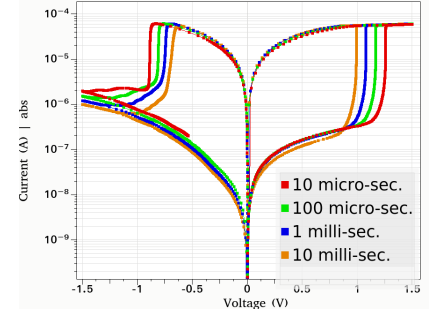


Fig. 5: Sweep time from 10 μs to 10 ms, ±1.5V, Tox = 4.5 nm

REFERENCES

- [1] A.Padovani *et al.*, NVMTS (2017), pp. 1-8.
- [2] Victory Device User's Manual by Silvaco International, (2023).
- [3] A.Padovani *et al.*, JAP 121 155101 (2017).
- [4] K.Muthuseenu *et al.*, SISPAD (2019), pp. 1-4.
- [5] W.Goes *et al.*, IMW 2021, pp. 17-20.
- [6] S.Deshmuk *et al.*, Sci.Adv. 8, eabk11514 (2022).
- [7] T.Sadi *et al.*, J.Phys: Cond.Mat. 30 (2018) 084005.
- [8] B.Traoré *et al.*, J.Phys.Chem.C 120, 43, pp 25023–25029 (2016).